Earthquake Engineering, Tenth World Conference © 1992 Balkema, Rotterdam. ISBN 90 5410 060 5

Inelastic modelling of backbone curve and hysteresis rules for low-rise R.C. perforated shear walls

J.-S. Yang & F.Y.Cheng
University of Missouri-Rolla, Mo., USA
M.S. Sheu
National Cheng-Kung University, Taiwan

ABSTRACT: A set of semi-empirical equations for backbone curve is formulated for the response behavior of low-rise non-boundary R.C. shear walls with openings subjected to lateral forces. These equations can be used to determine various loading capacities, displacements, and stiffnesses of crack, yield, ultimate,and failure stages. The hysteresis loops are developed with consideration of energy dissipation, opening size, opening location, and shear-span-length ratio. Hysteresis rules are formulated with all possible combinations of large and small amplitude loops. The formulation is based on both the experimental observation and analytical approaches. The comparison of calculated and experimental results is good.

1 INTRODUCTION

Shear walls without boundary elements are often used as seismic-resisting components in major civil engineering low-rise buildings and nuclear reactor category-I construction. A number of papers have been published on low-rise walls with boundary beams and columns; Cheng (1989) and Sheu (1988) have embarked on joint research of analytically and experimentally studying the walls without boundary elements. This paper presents recent research results of nonboundary low-rise R.C. walls with openings such as doors and windows. Walls having boundary elements and openings were studied by Yamada and Kawamura (1974) and Sato, Higashiura, et al. (1987), among other researchers.

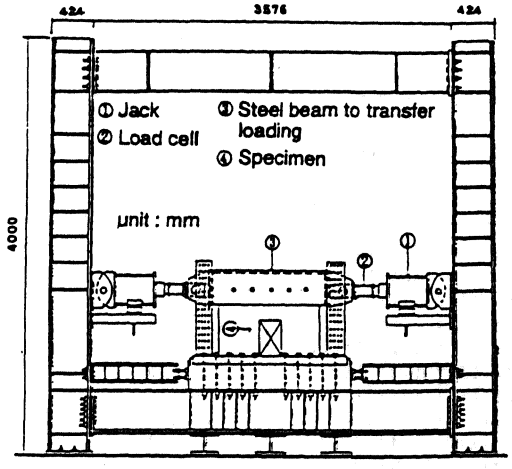

Figure 1. Test apparatus.

In this paper, the analytical studies are conducted at the University of Missouri-Rolla (UMR) on the basis of the experimental work performed at the National Cheng-Kung University (NCKU), Taiwan. Close collaboration is also undertaken with KAIST in Korea. The formulation has considered size and location of openings, horizontal and vertical steel bars, diagonal reinforcing bars around the openings, and shear-span-length ratio. The aforementioned factors are employed in deriving equations for calculating forces and displacements (load-deflection relationship) at various loading stages of cracking, yielding, ultimate, and failure. The load-deflection relationship (or backbone curve) is not only used to predict the resistance capacities of individual walls but also used in the analysis of hysteretic response of the walls. The hysteresis loops also include the parameters of energy dissipation, opening location, opening height, and shear-span-length ratio.

2 BACKBONE CURVE

2.1 Test specimens

There are two groups of wall elements with four types of openings used in the experimental study. Each type of wall elements is subjected to two kinds of loading history. One loading history is two-sided cyclic loading for the study of backbone curve. The other one is earthquake-type loading for hysteresis loops. Test apparatus is illustrated in Fig. 1. There is no boundary columns or girders around the wall element. The shear-span-length ratio is either 0.65 for group I wall elements or 0.9 for group II wall elements. The summary of seventeen wall elements and corresponding loading history is shown in Table 1.

Table 1. Specimen schedule and fundamental data.

Group ($\frac{L}{W}$)	Specimen no.	Specimen sketch	Opening size $N \times W_o \times L_o$	Steel bar: Vertical / Horizontal / Diagonal	f'_c (kg/cm^2)	Loading history
Group I (WxLxt : 100cmx50cmx10cm) 0.5	SW-0E			10-D10	254	
	SW-1E			5-D10	345	
	SW-2E			——	268	
	SWO-3E		1 × 21.8 × ** 37.5 (16.35%)	10-D10 / 5-D10 / D*-D13	299	
	SWO-4E				316	
	SWO-5E		2 × 21.8 × 18.75 (16.35%)	10-D10 / 5-D10 / D-D13	329	
	SWO-6E				329	
	SWO-7E		1 × 65.4 × 12.5 (16.35%)	10-D10 / 5-D10 / D-D13	328	
	SWO-8E				328	
Group II (WxLxt : 100cmx75cmx10cm) 0.75	SW-9E			10-D13 / 7-D13	294	
	SW-10E			——	312	
	SWO-11E		1 × 21.8 × 75.0 (21.8%)	8-D13 / 7-D13 / D-D13	297	
	SWO-12E				297	
	SWO-13E		2 × 21.8 × 37.5 (21.8%)	10-D13 / 7-D13 / D-D13	321	
	SWO-14E				325	
	SWO-15E		1 × 65.4 × 25.0 (21.8%)	10-D13 / 7-D13 / D-D13	279	
	SWO-16E				283	

* Diagonal bars ** Opening rate

The yielding stress of steel bars D10 and D13 are 5005 and 4617 kg/cm^2 respectively.

2.2 Observation of test results

In general, the wall element has larger displacement after element cracks than that in elastic range when it is subjected to same load increment due to its lower tensile strength of concrete.

Fig. 2(a) shows that when the crack occurs in the wall element, it results in a corresponding relative displacement Δ_1 of which the associated pseudo rotating center of crack (PRCC) is PRCC1. As the lateral loading increases, the crack extends to further rotating center PRCC2 with the corresponding displacement Δ_2 (Fig. 2(b)). Since the crack length L_{c2} is larger than L_{c1}, the displacement Δ_2 becomes larger (Fig. 2(c)). These diagonal cracks initiated at the beginning stage will form the main ones which control the behavior of wall element most because of the longest crack length and the associated largest crack

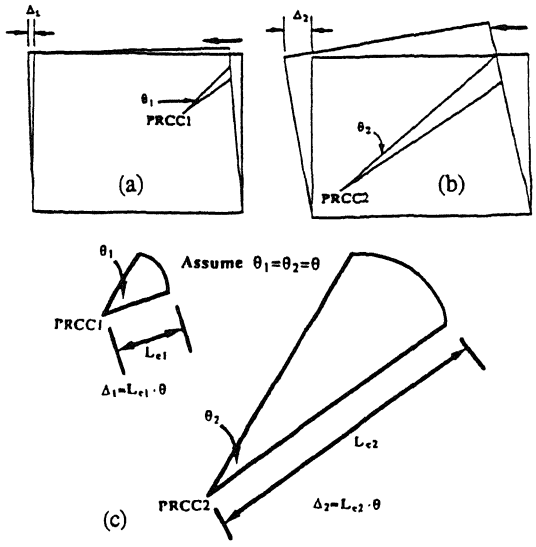

Figure 2. Development of diagonal crack.

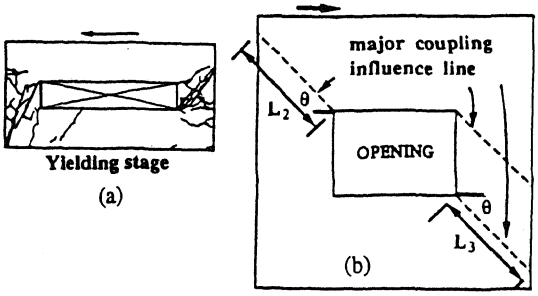

Figure 3. Crack development for SWO-7E.

width. This can be observed from Fig. 3(a). In this figure, diagonal cracks were developed and had larger crack width than that of the other cracks. These diagonal cracks result in large lateral displacement and restrict the lateral load capacity. For simplicity, the angle of main diagonal crack along the horizontal axis is assumed to be 45° to define critical(major) coupling influence line shown in Fig. 3(b). 'Critical' or 'major' here means that these diagonal cracks initiated at the earliest stage have wider crack width and longer crack length when comparing with that of the other cracks; coupling is the effect of combining flexural and shear strength. Most of diagonal cracks occur in the region underneath the major coupling influence line. Furthermore, if more diagonal cracks exist in the wall element, it may cause larger displacement. By knowing this, the effect of the horizontal steel bars is considered only underneath the top of openings. The fact from Fig. 3(a) is that the region just above the opening can be assumed to be elastic range since it does not have any crack, that is due to free end on the bottom side (or at the top of the opening). Therefore, it can be seen in Fig. 4 that this wedge-shaped region (assumed at crack

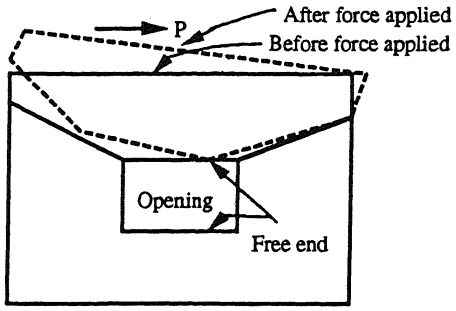

Figure 4. Wedge-shaped region.

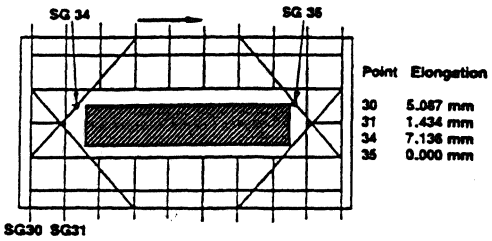

Figure 5. Elongation of diagonal bars for SWO-8E.

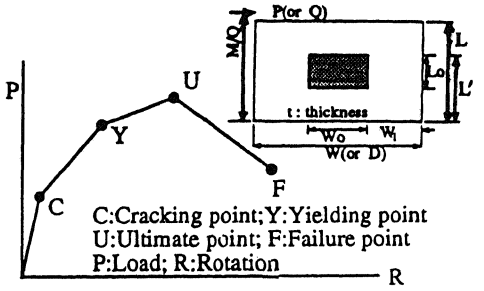

Figure 6. Critical points of backbone curve.

situation) can rotate and the vertical bars could yield along the crack on the both side of the wedge-shaped region. Based on this, the vertical bars are considered on the both side of opening through the overall length of the wall element.

Comparing the displacement from different strain gauges on the vertical bars and the diagonal bars from Fig. 5 (for the wall SWO-8E), it was found that the strain gauge SG34 for diagonal bars has large elongation (7.136 mm), and the strain gauge on the opposite side of loading point is 0.000 mm. That means the diagonal bar on the opposite side of loading point has little compression or tension; this phenomenon is also observed from other tests. Therefore, only the diagonal bars on the same side of loading point are considered. The lower diagonal bars on this side are also considered as they are located in tension. On the contrary, the lower diagonal bars on the opposite side of the loading point are neglected due to compression.

2.3 Semi-empirical equations

By using analytical derivation coupling with curve-fitting technique of experimental results, a set of equations has been developed for calculating forces and displacements at different loading stages. The force-displacement relationship or backbone curve is shown in Fig. 6 which includes the cracking (C), yielding (Y), ultimate (U), and failure (F) points. The derivation includes various effects of shear-span-length ratio MQD (=M/QD, M is the moment at the bottom of the wall), the height ratio of opening α_0(=L_0/L), the width ratio of opening β_0 (=W_0/W), the horizontal location factor of opening β_1 (=W_1/W), and vertical location factor of opening LWP (=L'/W_1) (see Fig. 6). The units used here are cm, kg and kg/cm^2. The equations of loading capacities and displacements corresponding to cracking, yielding, ultimate and failure stages are respectively listed in (a), (b), (c), and (d) in the following. Let

$$PWH=\left(\sum(\rho_{wh}f_y)\right)(L/W) \quad (1)$$

$$PWH1=\left(\sum(\rho_{wh}f_y/5000)\right)(L/W) \quad (2)$$

$$PWV=\left(\sum(\rho_{wv}f_y)\right)(W/L)^{\beta_1} \quad (3)$$

and

$$PWV1=\left(\sum(\rho_{wv}f_y/5000)\right)(W/L)^{\beta_2} \quad (4)$$

where ρ_{wh},ρ_{wv} represent the steel ratios of horizontal and vertical bars, respectively. For the loading capacities of individual walls, the equations are as follows.

(a) Cracking

$$P_c=\left[A_1+A_2(L'/L)(\alpha_0\beta_1)\right]\sqrt{f_c'}\,Wt \quad (5)$$

in which

$$A_1=0.0212+0.2762MQD \quad (6)$$

$$A_2=1.1531-1.2215MQD \quad (7)$$

(b) Yielding

$$P_y=\left[A_3+A_4\log_{10}\left[(L'/L)(\alpha_0\beta_1)\right]\right]P_u \quad (8)$$

in which

$$A_3=1.2657-0.3188MQD \quad (9)$$

$$A_4=0.2702-0.1362MQD \quad (10)$$

(c) Ultimate

$$P_u=\tau_u Wt \quad (11)$$

$$\tau_u=[U_1+U_2(L'/L)(\alpha_0\beta_1)]\sqrt{f_c'}+U_3\cdot PWH+U_4\cdot PWV \quad (12)$$

where

$$U_1=0.932-1.169MQD \quad (13)$$

$$U_2=-1.1741+1.5588MQD \quad (14)$$

$$U_3=0.3128-0.3249MQD \quad (15)$$

$$U_4=-0.1759+0.3079MQD \quad (16)$$

Here a_1 in PWV is 4.7663. The effects of horizontal bars $\sum(\rho_{wh}f_y)$ in PWH (or PWH1) and vertical bars $\sum(\rho_{wv}f_y)$ in PWV (or PWV1) will be discussed later

(d) Failure

$$P_f=(P_c+P_y)/2 \quad (17)$$

The displacements corresponding to the four loading stages are listed as follows.

(a) Cracking

$$D_c=C_1(F_{c1}+F_{c2}+F_{c3})(P_cL/GA_{og})\sqrt{f_c'/280} \quad (18)$$

in which

$$C_1=5.007-3.941MQD \quad (19)$$

$$F_{c1}=0.1775-9.61(L'/L)(W_1/W)(\alpha_0\beta_0) \quad (20)$$

$$F_{c2}=1903(PWV1) \quad (21)$$

$$F_{c3}=-1092(PWH1) \quad (22)$$

and

$$|F_{c1}+F_{c2}|>|F_{c3}| \quad (23)$$

$$A_{og}=(W-W_o)t+\sum_{i=1}^{NVB}(n_i-1)(A_v)_i \quad (24)$$

In Eq. 21, PWV1 is given in Eq. 4 where $a_2=-0.8418$

In Eq. (24) A_{og} is the transformed cross sectional area; NVB is the number of the vertical bars (Fig. 7);

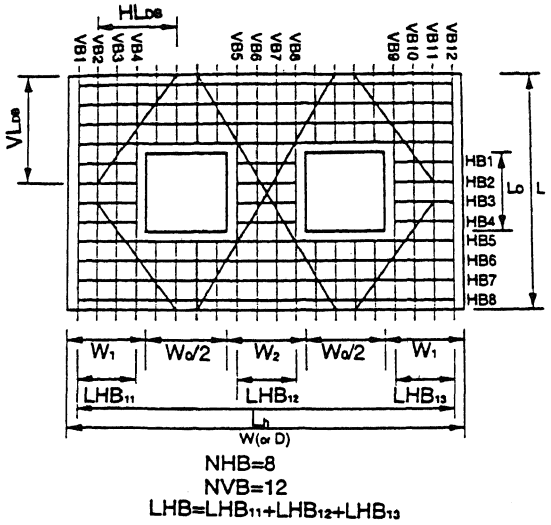

Figure 7. Number of vertical, horizontal bars considered in the calculation.

Table 2. Number of diagonal bars in calculation and f_r value.

WALL TYPE / COEFF										
NDB	1	2		3			4			
	DB1	DB1	DB2	DB1	DB2	DB3	DB1	DB2	DB3	DB4
f_r	0.5	0.5	1.00	0.5	1.00	1.00	0.5	1.00	0.5	1.00

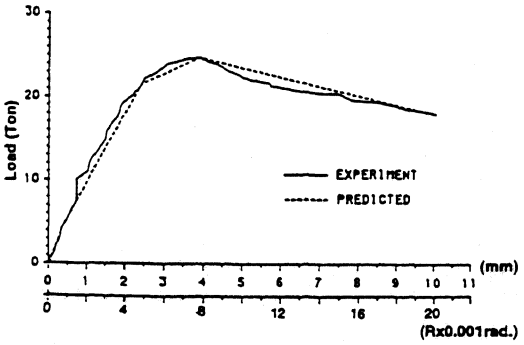

Figure 8. Comparison of experimental and calculated backbone curves for SWO-8E.

A_v is the cross sectional area of the vertical steel bar; and

$$n_i=\frac{E_s}{E_c}=\frac{\sigma_y/\varepsilon_{sy}}{15000\sqrt{f_c'}}=\frac{\sigma_y}{37.5\sqrt{f_c'}} \quad (25)$$

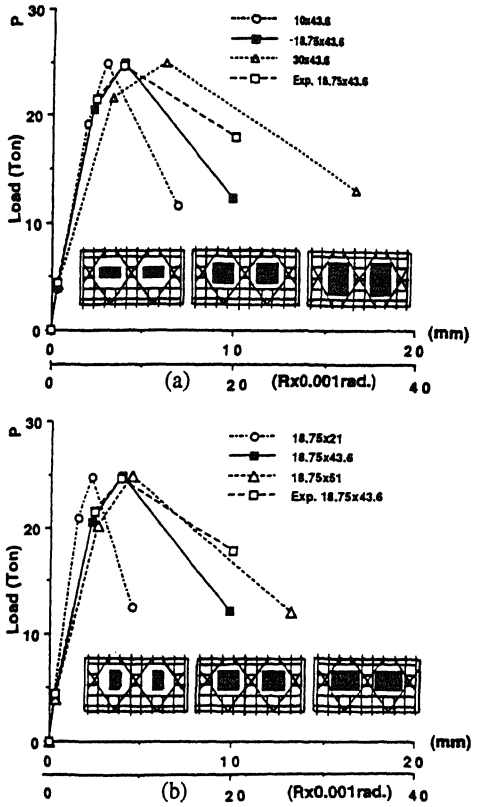

Figure 9. Comparison of backbone curves of different shear walls with openings.

where ε_{sy} is assumed to be 0.0025.

(b) Yielding

$$D_y=Y_1(F_{y1}+F_{y2}+F_{y3})(P_yL/GA_{og})/\sqrt{f_c'/280} \quad (26)$$

in which

$$Y_1=-1.878+3.773MQD \quad (27)$$

$$F_{y1}=7.697+229.2(L'/L)(W_1/W)(\alpha_0\beta_0) \quad (28)$$

$$F_{y2}=2622(PWV1) \quad (29)$$

$$F_{y3}=-6691(PWH1) \quad (30)$$

and

$$|F_{y1}+F_{y2}| > |F_{y3}| \quad (31)$$

Here a_2 in PWV1 is 0.6751.

(c) Ultimate

$$D_u=U_1(F_{u1}+F_{u2}+F_{u3})(P_uL/GA_{og})/\sqrt{f_c'/280} \quad (32)$$

in which

$$U_1=-0.7435+2.4MQD \quad (33)$$

$$F_{u1}=13.05+488.6(L'/L)(W_1/W)(\alpha_0\beta_0) \quad (34)$$

$$F_{u2}=2214(PWV1) \quad (35)$$

$$F_{u3}=-7685(PWH1) \quad (36)$$

and

$$|F_{u1}+F_{u2}| > |F_{u3}| \quad (37)$$

Here a_2 in PWV1 is 0.2997.

(d) Failure

$$D_f=(C_{f1}+C_{f2}(LWP))D_u \quad (38)$$

in which

$$C_{f1}=2.2349-3.4173MQD \quad (39)$$

$$C_{f2}=1.5608-0.4736MQD \quad (40)$$

In Eqs. (1) to (4), $\sum(\rho_{wh}f_y)$ and $\sum(\rho_{wv}f_y)$ are defined as

$$\sum(\rho_{wh}\sigma_y)=\frac{1}{Lt}(EHB)+\frac{1}{Lt}(EDBH) \quad (41)$$

$$\sum(\rho_{wv}f_y)=\frac{1}{Wt}(EVB)+\frac{1}{Wt}(EDBV) \quad (42)$$

where

$$EHB=\sum_{i=1}^{NHB}((A_h)_i(f_y)_i(f_{lhh})_i) \quad (43)$$

$$EDBH=\sum_{i=1}^{NDB}((A_d)_i(f_y)_i(f_{adh})_i(f_{ldh})_i(f_r)_i) \quad (44)$$

$$EVB=\sum_{i=1}^{NVB}((A_v)_i(f_y)_i) \quad (45)$$

$$EDBV=\sum_{i=1}^{NDB}((A_d)_i(f_y)_i(f_{adv})_i(f_{ldv})_i(f_r)_i) \quad (46)$$

$$(f_{lhh})_i=(LHB)_i/L_h \quad (47)$$

$$(f_{adh})_i=(HB_{DB})_i/\sqrt{(HL_{DB})_i^2+(VL_{DB})_i^2} \quad (48)$$

$$(f_{ldh})_i=(HL_{DB})_i/L_h \quad (49)$$

$$(f_{ldv})_i=(VL_{DB})_i/L_h \quad (50)$$

Table 3. Summary of hysteresis rules.

	|Dmax|<Dc	Dc<|Dmax|<Dy	Dy<|Dmax|
(a)	● K=0SOC, (11*)	● K=0SCY** or SCY, (211)	● if Dc<|DP|<Dy, K=SCY, (3121) ● if Dy<|DP|<Du, K=0SYU or SYU, (3111) ● if Du<|DP|, K=SUP, (3112)
(b)	● K=0SOC, (112)	1. Keyfs<0.7Fyo ● if Fc/3<|FP|<0.7Fyo, K=SOC, (2211) ● if |FP|<FC/3, K=STC', (2212) (if K>SOC, K=Ka) 2. Keyfs>0.7Fyo ● K=Kd, (2221) ● K=max(SHC', SOB), (2222) ● K=SHY', (2223) (if SHY'<SNO, K=1.5SNO)	● K=Kd, (321) ● K=SOB, (3221) ● if Dmax<1.6Duo, K=SNY', (3231) ● if Dmax>1.6Duo, K=SNC', (3232)
(c)	● if Xo=0, K=0SOC, (11) ● if Xo=0, K=SXoC', (131) (above for Keyds>Dc) ● if Keyds<Dc, K=Ka, (1313)	● if DM<0.75Duo, K=SXoC', (2312) (if Keyds<Dc, K=Ka, (2313)) ● if DM>0.75Duo, K=SR, (231)	● if DM<0.75Duo, K=SXoC', (3412) (if Keyds<Dc, K=Ka, (3413) ● if DM>0.75Duo, K=SR, (341)
(d)		● K=Kb, (251) ● K=0.5Kb, (252)	● K=Kb, (331) ● K=0.2Kb, (332)

NOTE: For small amplitude loop
● K=Ke, (241)
● K=Kf, (242)
● K=Kg=0.4Kf, (242) (if DM<0.75Duo, K=Kg=SCY)

* rule number
** if no energy dissipation
C', Y': cracking pt., and yielding pt. in the opposite side
DM: max. displ. before current cycle

DP: current displ.
Original backbone curve uses 0SOC, 0SCY, etc.
Reference curve uses SOC, SCY, etc.
Kd, Ke: verticle line

(a) Loading (b) Unloading (c) Reversal loading (d) Reloading after unloading

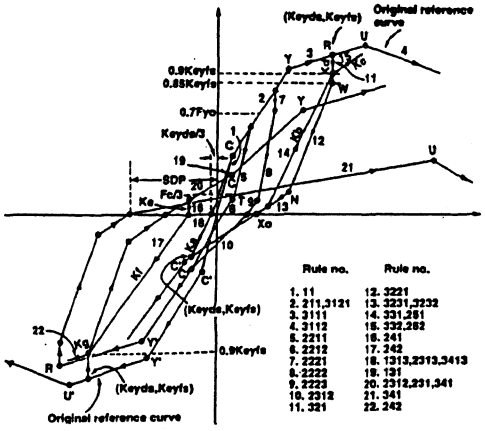

Figure 10. Hysteresis loops.

$$(f_{adv})_i=(VL_{DB})_i/\sqrt{(HL_{DB})_i^2+(VL_{DB})_i^2} \qquad (51)$$

Determination of f_r is shown in Table 2.

2.4 Comparison of results and discussions

Fig. 8 shows the comparison between experimental data and calculated results of wall SWO-6E, the difference is very small. The comparisons of load-displacement curves for various opening sizes are shown in Fig. 9. In Fig. 9(a), the width of each opening of the three walls is 43.6 cm but opening height varies. It shows that the wall with larger opening height has larger deflection at failure stage but not much difference at crack and yield. In Fig. 9(b), the opening height in each wall is 18.75 cm, but the opening width varies. The wall having larger opening width suffers more deflection, but negligible difference at crack, slight difference at yield. All these curves are compared with the experimental results of wall SWO-6E.

3 HYSTERESIS MODEL

The hysteresis rules are controlled by displacement in this model. From Table 3, D_{max} is defined as the maximum displacement in current cycle. The cycle means the force must undergo positive and negative phases with displacement at the same side, and then go back to zero force. The general hysteresis rules shown in Fig. 10 represent the behavior of a shear wall with opening and are highly related to the shear-span-length ratio (MQD), opening location factor (LWP), opening height ratio (α_0), and energy dissipation factor $\left(\sum E_d/(F_{uo}D_{uo})\right)$, where $\sum E_d$ is the summation of the energy dissipation; F_{uo} and D_{uo} are the ultimate load and ultimate displacement of the original backbone curve, respectively. The comparison between test results and predicted responses is shown in Fig. 11; the curve predicted is very close to the experimental response of wall SWO-8E.

4 CONCLUSIONS

In this paper, the equations of the backbone curve and the hysteresis rules of low-rise non-boundary shear walls with openings are established. The comparisons of predicted response and experimental results at various loading stages of cracking, yielding, ultimate, and failure are good. The load capacity and deflection

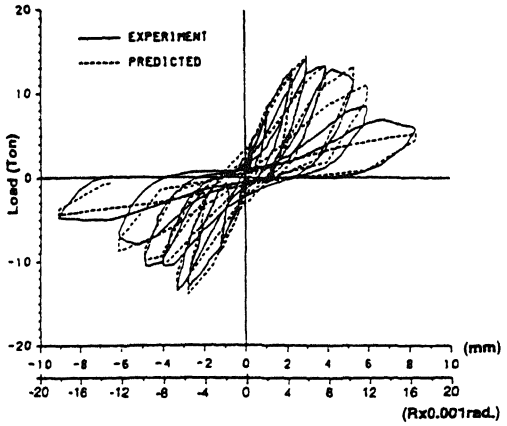

Figure 11. Comparison of experimental and calculated hysteretic responses for SWO-8E.

equations as well as the hysteresis model proposed here can accurately predict the response behavior of structural systems with perforated shear walls.

ACKNOWLEDGMENTS

This paper is based on a joint research project between UMR (USA), NCKU (Taiwan), and KAIST (Korea) for which UMR's work is supported by the NSF Grants BCS-9001494 and INT 891284. The computer time is provided by the Center for Theory and Simulation in Science and Engineering at Cornell University. All the support is gratefully acknowledged.

REFERENCES

Cheng, F. Y. and Mertz, G. E. 1989. Inelastic seismic response of reinforced-concrete low-rise shear walls and building systems, final report 89-30 prepared for the National Science Foundation.

Sato, Y., A. Higashiura, et al. 1987. Load-deflection characteristics of shear walls with openings. *Proc. 9th Int. Conference on Structural Mechanics in Reactor Technology*, Lausanne. Vol. H: 537-542.

Sheu, M. S. 1988. Behavior of low-rise shear walls subjected to reversed cycling loading, Technical report to the National Science Council, Taiwan.

Yamada, M., H. Kawamura & K.Katagihara 1974. Reinforced concrete shear walls with openings. *Shear in reinforced concrete*, SP-42, Vol. 2, ACI.